CORONAVIRUS

An engineered decoy receptor for SARS-CoV-2 broadly binds protein S sequence variants

Kui K. Chan[1], Timothy J. C. Tan[2], Krishna K. Narayanan[2], Erik Procko[2]*

The spike S of SARS-CoV-2 recognizes ACE2 on the host cell membrane to initiate entry. Soluble decoy receptors, in which the ACE2 ectodomain is engineered to block S with high affinity, potently neutralize infection and, because of close similarity with the natural receptor, hold out the promise of being broadly active against virus variants without opportunity for escape. Here, we directly test this hypothesis. We find that an engineered decoy receptor, $sACE2_2$.v2.4, tightly binds S of SARS-associated viruses from humans and bats, despite the ACE2-binding surface being a region of high diversity. Saturation mutagenesis of the receptor-binding domain followed by in vitro selection, with wild-type ACE2 and the engineered decoy competing for binding sites, failed to find S mutants that discriminate in favor of the wild-type receptor. We conclude that resistance to engineered decoys will be rare and that decoys may be active against future outbreaks of SARS-associated betacoronaviruses.

INTRODUCTION

Zoonotic coronaviruses have crossed over from animal reservoirs multiple times in the past two decades, and it is almost certain that wild animals will continue to be a source of devastating outbreaks. Unlike ubiquitous human coronaviruses responsible for common respiratory illnesses, these zoonotic coronaviruses with pandemic potential cause serious and complex diseases, partly due to their tissue tropisms driven by receptor usage. Severe acute respiratory syndrome coronaviruses 1 (SARS-CoV-1) and 2 (SARS-CoV-2) engage angiotensin-converting enzyme 2 (ACE2) for cell attachment and entry (*1*–*7*). ACE2 is a protease responsible for regulating blood volume and pressure that is expressed on the surface of cells in the lung, heart, and gastrointestinal tract, among other tissues (*8*, *9*). The ongoing spread of SARS-CoV-2 and the disease it causes, coronavirus disease 2019 (COVID-19), has had a crippling toll on global healthcare systems and economies, and effective treatments and vaccines are urgently needed.

As SARS-CoV-2 becomes endemic in the human population, it has the potential to mutate and undergo genetic drift and recombination. To what extent this will occur as increasing numbers of people are infected and mount counter immune responses is unknown, but already a variant in the viral spike protein S (D614G) has rapidly emerged from multiple independent events and effects S protein stability and dynamics (*10*, *11*). Another S variant (D839Y) became prevalent in Portugal, possibly due to a founder effect (*12*). SARS-CoV-2 has a moderate mutation rate estimated at 10^{-3} substitutions per site per year (*13*). However, the virus has undergone rapid mutation and adaptation after infecting mink in Denmark, from which it then crossed back to humans (*14*), causing Danish authorities to order 17 million farmed mink culled to preemptively prevent the possible emergence of vaccine-resistant variants. In addition, large changes in coronavirus genomes have frequently occurred in nature from recombination events, especially in bats where coinfection levels can be high (*15*, *16*). Recombination of Middle East respiratory syndrome CoVs has been documented in camels (*17*); there are reported cases of recombination between cocirculating SARS-CoV-2 variants (*18*), and SARS-CoV-2 itself may have emerged through recombination of coronavirus genomes (*19*). This will all have profound implications for the current pandemic's trajectory, the potential for future coronavirus pandemics, and whether drug or vaccine resistance in SARS-CoV-2 emerges and becomes widespread.

The viral spike is a vulnerable target for neutralizing monoclonal antibodies that are progressing through clinical trials, yet in tissue culture, escape mutations in the spike rapidly emerge to all antibodies tested (*20*). Deep mutagenesis of the isolated receptor-binding domain (RBD) by yeast surface display has easily identified mutations in S that retain high expression and ACE2 affinity but are no longer bound by monoclonal antibodies and confer resistance (*21*). This has motivated the development of cocktails of noncompeting monoclonals (*20*, *22*), inspired by lessons learned from the treatment of HIV-1 and Ebola, to limit the possibilities for the virus to escape. Notably, drugmaker Eli Lilly has a monoclonal monotherapy (LY-CoV555) in advanced trials (NCT04427501) where the selection of resistant virus variants in patients has occurred. A trial update added an arm with a second monoclonal (LY-CoV016), and the company has not reported putative resistance variants in patients receiving the cocktail thus far. However, even the use of monoclonal cocktails does not address future coronavirus spillovers from wild animals that may be antigenically distinct. Large screening efforts were required to find antibodies from recovered patients with SARS-CoV-1 that cross-react with SARS-CoV-2 (*23*), indicating that antibodies have confined capacity for interacting with variable epitopes on the spike surface and are unlikely to be broad and pan-specific for all SARS-related viruses.

An alternative protein-based antiviral to monoclonal antibodies is to use soluble ACE2 (sACE2) as a decoy to compete for receptor-binding sites on the viral spike (*6*, *24*–*27*). In principle, the virus has limited potential to escape sACE2-mediated neutralization without simultaneously decreasing affinity for the native ACE2 receptor, rendering the virus less virulent. Wild-type (WT) sACE2 is currently in a phase 2 clinical trial (*28*), and multiple groups have now engineered sACE2 to create high-affinity decoys for SARS-CoV-2 that rival matured monoclonal antibodies for potent neutralization of infection (*27*, *29*, *30*). In our group, deep mutagenesis was used to identify a large number of mutations in ACE2 that increase affinity for S (*27*). These mutations were dispersed across the interface and

[1]Orthogonal Biologics, Champaign, IL 61821, USA. [2]Department of Biochemistry and Cancer Center at Illinois, University of Illinois, Urbana, IL 61801, USA.
*Corresponding author. Email: procko@illinois.edu

also at distal sites where they are predicted to enhance folding of the virus-recognized conformation. A combination of three mutations, called sACE2$_2$.v2.4, increases affinity by 35-fold and binds SARS-CoV-2 S [dissociation constant (K_D), 600 pM] with affinity comparable to the best monoclonal antibodies (*27*). Even tighter apparent affinities are reached through avid binding to trimeric spike expressed on a membrane. Despite engineering being focused exclusively on SARS-CoV-2 affinity, sACE2$_2$.v2.4 potently neutralized authentic SARS-CoV-1 and SARS-CoV-2 infection in tissue culture, suggesting that its close resemblance to the WT receptor confers broad activity against ACE2-utilizing betacoronaviruses generally. sACE2$_2$.v2.4 is dimeric and monodisperse without aggregation, catalytically active, highly soluble, stable after storage at 37°C for days, and well expressed at levels greater than the WT protein. Because of both its high activity and favorable properties for manufacture, sACE2$_2$.v2.4 is a genuine drug candidate for preclinical development.

Engineered, high-affinity decoy receptors, while very similar to natural ACE2, nonetheless have mutations present at or near the interaction surface. There is therefore an opportunity for viral spike variants to discriminate between an engineered decoy and WT receptors, providing a route toward resistance. Here, we show that the engineered decoy sACE2$_2$.v2.4 binds broadly and tightly to the RBDs of diverse SARS-associated betacoronaviruses that use ACE2 for entry. We further fail to find mutations within the RBD, which directly contacts ACE2 and is where possible escape mutations will most likely reside, that redirect specificity toward the WT receptor. We conclude that resistance to an engineered decoy receptor will be rare, and sACE2$_2$.v2.4 targets common attributes for affinity to S in SARS-associated viruses.

RESULTS

An engineered decoy receptor broadly binds RBDs from SARS-associated CoVs with tight affinity

The affinities of the decoy receptor sACE2$_2$.v2.4 were determined for purified RBDs from the S proteins of five coronaviruses from *Rhinolophus* bat species (isolates LYRa11, Rs4231, Rs7327, Rs4084, and RsSHC014) and two human coronaviruses, SARS-CoV-1 and SARS-CoV-2. These viruses fall within a common clade of betacoronaviruses that have been experimentally validated to use human ACE2 as an entry receptor (*7*). They share close sequence identity within the RBD core, while variation is highest within the functional ACE2-binding site (Fig. 1 and fig. S1), possibly due to a coevolutionary "arms race" with polymorphic ACE2 sequences in ecologically diverse bat species (*31*). Affinity was measured by biolayer interferometry (BLI), with sACE2$_2$ [amino acids (a.a.) S19 to G732] fused at the C terminus with the Fc moiety of human immunoglobulin G1 (IgG1) immobilized to the sensor surface and monomeric 8his-tagged RBD (fig. S2) used as the soluble analyte. This arrangement excludes avidity effects, which otherwise cause artificially tight (picomolar) apparent affinities whenever dimeric sACE2$_2$ in solution is bound to immobilized RBD decorating an interaction surface. WT sACE2$_2$ bound all the RBDs with affinities ranging from 16 nM for SARS-CoV-2 to 91 nM for LYRa11, with a median affinity of 60 nM (Table 1). The measured affinities for the RBDs of SARS-CoV-1 and SARS-CoV-2 are comparable to those of published data (*4*, *27*, *32*–*34*). Engineered sACE2$_2$.v2.4 displayed large increases in affinity for all the RBDs, with K_Ds ranging from 0.4 nM for SARS-CoV-2 to 3.5 nM for the isolate Rs4231, with a median affinity less than 2 nM (Table 1).

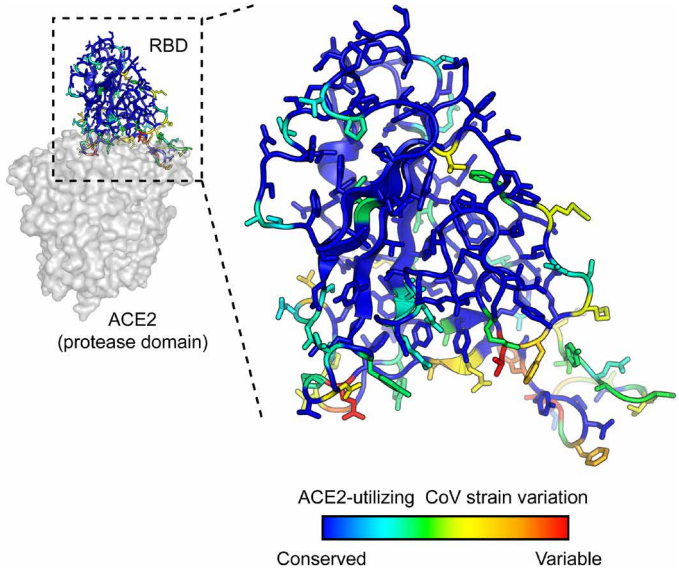

Fig. 1. SARS-associated coronaviruses have high sequence diversity at the ACE2-binding site. The RBD of SARS-CoV-2 [Protein Data Bank (PDB): 6M17] is colored by diversity between seven SARS-associated CoV strains (blue, conserved; red, variable).

The approximate 35-fold affinity increase in the engineered decoy applies universally to coronaviruses in the test panel, and the molecular basis for affinity enhancement must therefore be grounded in common attributes of RBD/ACE2 recognition.

A deep mutational scan of the RBD in the context of full-length S reveals that residues in the ACE2-binding site are mutationally tolerant

To explore potential sequence diversity in S of SARS-CoV-2 that may act as a "reservoir" for drug resistance, we evaluated the mutational tolerance of the RBD by deep mutagenesis (*35*). Saturation mutagenesis was focused to the RBD (a.a. C336 to L517) of full-length S tagged at the extracellular N terminus with a c-myc epitope for detection of surface expression. The spike library, encompassing 3640 single amino acid substitutions, was transfected in human Expi293F cells under conditions where cells typically acquire no more than a single sequence variant (*36*, *37*). The culture was incubated with WT, 8his-tagged, dimeric sACE2$_2$ at a subsaturating concentration (2.5 nM). Bound sACE2$_2$-8h and surface-expressed S were stained with fluorescent antibodies for flow cytometry analysis (Fig. 2A). Compared to cells expressing WT S, the library was poorly expressed, indicating that many mutations are deleterious for folding and expression. A cell population was discernable expressing S variants that bind ACE2 with decreased affinity (Fig. 2B). After gating for c-myc–positive cells expressing S, cells with high and low levels of bound sACE2$_2$ were collected by fluorescence-activated cell sorting (FACS), called the ACE2-high and ACE2-low populations, respectively (Fig. 2C). Both the expression and sACE2$_2$-binding signals decreased over minutes to hours during sorting, possibly due to shedding of the S1 subunit. Cells were therefore collected and pooled from three separate FACS experiments for a combined 8-hour sort time.

Transcripts in the sorted cells were Illumina sequenced and compared to the naïve plasmid library to determine an enrichment ratio for each amino acid substitution (*38*). Mutations in S that

Table 1. BLI kinetics for immobilized sACE2$_2$-IgG1 binding to coronavirus RBDs.

CoV strain*	WT sACE2$_2$-IgG1†				sACE2$_2$.v2.4-IgG1			
	k_{on} (M^{-1} s^{-1})	k_{off} (s^{-1})	K_D (nM)	χ^{2}‡	k_{on} (M^{-1} s^{-1})	k_{off} (s^{-1})	K_D (nM)	χ^{2}
LYRa11	8.7×10^{5}	7.9×10^{-2}	91	0.12	1.4×10^{6}	2.5×10^{-3}	1.8	0.10
Rs7327	6.4×10^{5}	4.0×10^{-2}	63	0.25	9.8×10^{5}	1.8×10^{-3}	1.9	0.11
Rs4231	3.2×10^{5}	2.2×10^{-2}	69	0.04	4.5×10^{5}	1.6×10^{-3}	3.5	0.10
Rs4084	2.9×10^{5}	2.5×10^{-2}	85	0.24	4.8×10^{5}	1.5×10^{-3}	3.1	0.10
RsSHC014	8.8×10^{5}	2.6×10^{-2}	29	0.20	1.6×10^{6}	2.0×10^{-3}	1.3	0.29
SARS-1	6.6×10^{3}	1.2×10^{-4}	58	0.03	3.0×10^{3}	5.6×10^{-6}	2.1	0.03
SARS-2	1.4×10^{6}	8.1×10^{-3}	16	0.25	6.6×10^{5}	2.8×10^{-4}	0.4	0.09
SARS-2 (Y449K)	2.0×10^{6}	9.0×10^{-2}	46	0.67	4.3×10^{6}	4.0×10^{-3}	0.9	0.71
SARS-2 (N501W)	2.4×10^{6}	5.4×10^{-3}	2.3	0.43	3.3×10^{6}	2.8×10^{-4}	0.1	0.23
SARS-2 (N501Y)	2.2×10^{6}	1.8×10^{-3}	0.8	0.15	3.6×10^{5}	1.1×10^{-4}	<0.1	0.24

*Purified RBDs at five to seven concentrations were used as the soluble analytes. †IgG1 Fc–fused sACE2$_2$ was immobilized to anti-human IgG Fc capture biosensors. ‡χ^2 values represent the goodness of curve fitting. Acceptable values were considered to be less than 3.

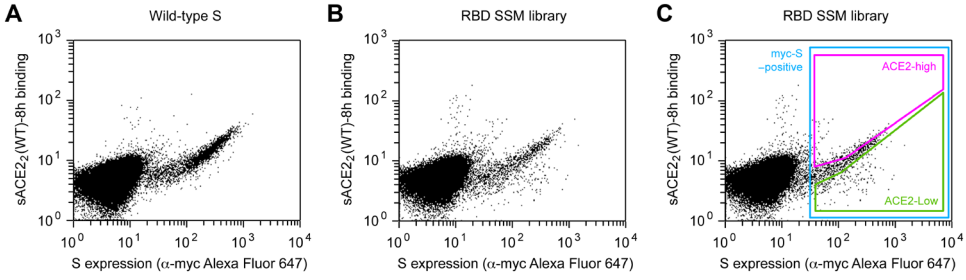

Fig. 2. FACS selection for variants of S with high or low binding signal to ACE2. (**A**) Flow cytometry analysis of Expi293F cells expressing full-length S of SARS-CoV-2 with an N-terminal c-myc tag. Staining for the myc-epitope is on the *x* axis, while the detection of bound sACE2$_2$-8h (2.5 nM) is on the *y* axis. S plasmid was diluted 1500-fold by weight with carrier DNA so that cells typically express no more than one coding variant; under these conditions, most cells are negative. (**B**) Flow cytometry of cells transfected with the RBD single site-saturation mutagenesis (SSM) library shows cells expressing S variants with reduced sACE2$_2$-8h binding. (**C**) Gating strategy for FACS. S-expressing cells positive for the c-myc epitope were gated (blue), and the highest ("ACE2-high") and lowest ("ACE2-low") 20% of cells with bound sACE2$_2$-8h relative to myc-S expression were collected.

express and bind ACE2 tightly are selectively enriched in the ACE2-high sort (fig. S3); mutations that express but have reduced ACE2 binding are selectively enriched in the ACE2-low sort; and mutations that are poorly expressed are depleted from both sorted populations. Positional conservation scores were calculated by averaging the $\log_2$ enrichment ratios for each of the possible amino acids at a residue position. By adding conservation scores for both the ACE2-high and ACE2-low sorts, we derive a score for surface expression, which shows that the hydrophobic RBD core is tightly conserved for folding and trafficking of the viral spike (Fig. 3A). By comparison, residues on the exposed RBD surface are mutationally permissive for S surface expression. This matches the mutational tolerance of proteins generally.

For tight ACE2 binding (i.e., S variants in the ACE2-high population), conservation increases for RBD residues at the ACE2 interface, yet mutational tolerance remains high (Fig. 3C). The sequence diversity observed among natural betacoronaviruses, which display high diversity at the ACE2-binding site, is therefore replicated in the deep mutational scan, which predicts that the SARS-CoV-2 spike tolerates substantial genetic diversity at the receptor-binding site for function. From this accessible sequence diversity, SARS-CoV-2 might feasibly mutate to acquire resistance to monoclonal antibodies or engineered decoy receptors targeting the ACE2-binding site.

There are two "hotspot" regions for interactions at the interface that determine receptor affinity and species adaptation, centered around ACE2 residues K31 and K353 (*39*). These regions are also the locations for substitutions to ACE2 residues T27, L79, and N330 in the engineered sACE2$_2$.v2.4 decoy. Mutations to RBD residues at these sites tend to be weakly depleted for high ACE2 binding (fig. S4) but are much more tolerant of mutations than structural positions buried in the RBD core. To highlight a few residues, S-Y505 that packs against the hydrocarbon chain of ACE2-K353 is notably more conserved than most other interfacial residues, with the exceptions of partially buried residues like S-R403 and S-Y453 that likely have additional structural roles; S-Y489 contacting ACE2-T27 and ACE2-K31 has an overall weak preference for aromatic amino acids; and S-G485 on a loop packed against ACE2-L79 has its highest tolerance for polar substitutions, possibly to maintain the loop conformation and solubility (fig. S4). Some mutations are found to be highly enriched for ACE2 binding, including small hydrophobic amino acids for S-Q493 and aromatic amino acids for S-N501 that are both anticipated to increase local hydrophobic or aromatic ring packing. This is consistent with observations from yeast surface display of RBD mutants (*40*). The S-N501Y mutation, which causes a notable increase in affinity for ACE2 (Table 1), has emerged in a

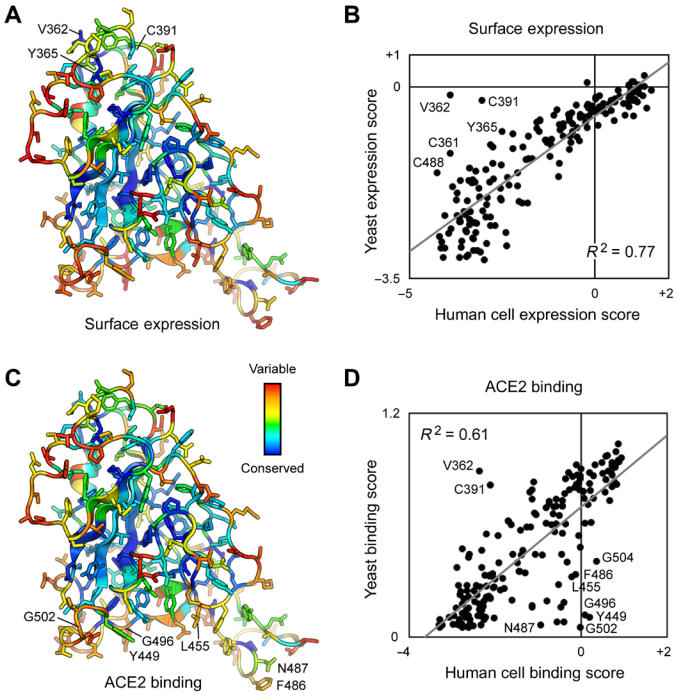

Fig. 3. Deep mutagenesis reveals that the ACE2-binding site of SARS-CoV-2 tolerates many mutations. (**A**) Positional scores for surface expression are mapped to the structure of the SARS-CoV-2 RBD (PDB: 6M17, oriented as in Fig. 1). Blue residues in the protein core are highly conserved in the FACS selection for surface S expression (judged by depletion of mutations from the ACE2-high and ACE2-low gates), while surface residues in red tolerate mutations. (**B**) Correlation plot of expression scores from mutant selection in human cells of full-length S (*x* axis) versus the conservation scores (mean of the $\log_2$ enrichment ratios at a residue position) from mutant selection in the isolated RBD by yeast display (*y* axis). Notable outliers are indicated. (**C**) Conservation scores from the ACE2-high gated cell population are mapped to the RBD structure, with residues colored from low (blue) to high (red) mutational tolerance. (**D**) Correlation plot of RBD conservation scores for high ACE2 binding from deep mutagenesis of S in human cells (*x* axis) versus deep mutagenesis of the RBD on the yeast surface (mean of $\Delta K_{D\ app}$; *y* axis).

highly transmissible SARS-CoV-2 variant (B.1.1.7) originating in England (*41*).

Comparison to a deep mutational scan of the isolated RBD by yeast surface display

Two deep mutational scans have been reported for the isolated RBD displayed on the surface of yeast (*40*, *42*). We compare our data from a selection of full-length S expressed in human cells to the publicly accessible Starr *et al.* dataset (*40*). Important residues within the RBD for surface expression of full-length spike in human cells are closely correlated with data from yeast surface display of the isolated RBD (Fig. 3B), with the exception of a notable region. The surface of the RBD opposing the ACE2-binding site (e.g., V362, Y365, and C391) is free to mutate for yeast surface display, but its sequence is constrained in our experiments; this region of the RBD is buried by connecting structural elements to the global fold of an S subunit in the closed-down conformation (this is the dominant conformation for S subunits and is inaccessible to receptor binding; fig. S5) (*2*, *4*, *43*, *44*). While some mutations might have allosteric effects, we note that among substitutions of V362, Y365, and C391, mutations tend to be lightly depleted from the ACE2-low and heavily depleted from the ACE2-high sorted populations. No mutations at these positions were selectively enriched in just the ACE2-high sort, as might be expected if a mutation favored the open-up conformation through allosteric mechanisms. This is consistent with mutations at these residues reducing ACE2 interactions through defects in folding and decreased surface expression. Compared to single mutations that destabilize the RBD in the closed-down conformation, more extensive engineering with multiple stabilizing mutations has been shown to shift the conformational equilibrium of S subunits to the open-up state (*45*).

We used targeted mutagenesis to individually test alanine substitutions to all the cysteines in the RBD (fig. S5). We found that all cysteine-to-alanine mutations severely diminish S surface expression in Expi293F cells, including C391A and C525A on the RBD "backside" that were neutral in the yeast display scan (*40*). These differences demonstrate that there are tighter sequence constraints on the RBD in the context of a full spike expressed at a human cell membrane, yet overall, we consider the yeast display and the human cell datasets to closely agree.

For binding to dimeric $sACE2_2$, we note that interface residues were more tightly conserved in the Starr *et al.* dataset (Fig. 3D), possibly a consequence of three differences between the deep mutagenesis experiments. First, our selections for ACE2 binding of S variants at the plasma membrane appear to primarily reflect mutational effects on surface expression, which is almost certainly more stringent in human cells. Yeast permits many poorly folded proteins to leak to the cell surface (*46*). Second, the yeast selections were conducted at multiple sACE2 concentrations from which apparent K_D changes were computed (*40*); the Starr *et al.* dataset in this regard is very comprehensive. Because of the long sort times required for our human cell libraries where only a small fraction of cells express spike, we sorted at a single $sACE2_2$ concentration that cannot accurately capture a range of different binding affinities quantitatively. Third, dimeric $sACE2_2$ may geometrically complement trimeric S densely packed on a human cell membrane, such that avidity masks the effects of affinity-reducing mutations. Nonetheless, there is overall agreement that ACE2 binding often persists following mutations to the RBD surface, and our data simply suggest that mutational tolerance may be even greater than that already observed by Starr *et al.*

A screen for S variants that preferentially bind WT ACE2 over the engineered decoy

Having shown that the ACE2-binding site of SARS-CoV-2 protein S tolerates many mutations, we asked whether mutations might therefore be found that confer resistance to the engineered decoy $sACE2_2$.v2.4. Resistance mutations are anticipated to lose affinity for $sACE2_2$.v2.4 while maintaining binding to the WT receptor and are most likely to reside in the RBD where physical contacts are made. Similar reasoning formed the foundation of a deep mutagenesis–based selection of the isolated RBD by yeast surface display to find escape mutations to monoclonal antibodies, and the results were predictive of escape mutations in pseudovirus growth selections (*21*).

To address whether escape mutations from the engineered decoy might be found in the RBD, we repurposed the S protein library for a specificity selection. Cells expressing the library, encoding all possible substitutions in the RBD, were coincubated with WT $sACE2_2$ fused to the Fc region of IgG1 and 8his-tagged $sACE2_2$.v2.4 at concentrations where both proteins bind competitively (*27*). It was

immediately apparent from flow cytometry of the Expi293F culture expressing the S library that there were cells expressing S variants shifted toward preferential binding to sACE2$_2$.v2.4, but no substantial population with preferential binding to the WT receptor (Fig. 4, A and B). Cells expressing S variants that might preferentially bind sACE2$_2$(WT)-IgG1 or sACE2$_2$.v2.4 were gated and collected by FACS (Fig. 4C), followed by deep sequencing of S transcripts to determine enrichment ratios. There was close agreement between two independent replicate experiments (Fig. 4, D to G). Most RBD mutations were depleted following sorting, consistent with deleterious effects on S folding and expression.

sACE2$_2$.v2.4 has three mutations from WT ACE2: T27Y buried within the RBD interface and L79T and N330Y at the interface periphery (Fig. 5A). A substantial number of mutations in the RBD of S were selectively enriched for preferential binding to sACE2$_2$.v2.4 (Fig. 5B, upper left quadrant). While sACE2$_2$.v2.4-specific mutations could be found immediately adjacent to the sites of engineered mutations in ACE2 (particularly mutations to S-F486 adjacent to ACE2-L79 and S-T500 adjacent to ACE2-N330), major hotspots for sACE2$_2$.v2.4-specific mutations were also mapped to RBD loops 498 to 506, contacting the region where the ACE2-α1 helix packs against a β-hairpin motif (Fig. 5A). By comparison, there were no hotspots in the RBD for sACE2$_2$(WT)-specific mutations. Only a small number of mutations were selectively enriched for preferential binding to WT receptor (Fig. 5B), and the abundance of these putative WT-specific mutations barely rose above the expected level of noise in the deep mutagenesis data. In this competition assay, S binding to WT sACE2$_2$ is therefore more sensitive to RBD mutations than S binding to engineered sACE2$_2$.v2.4.

To determine whether the potential WT ACE2–specific mutations found by deep mutagenesis are real as opposed to false predictions due to data noise, we tested 24 mutants of S selectively enriched in the WT-specific gate by targeted mutagenesis (blue data points in Fig. 5B). Only minor shifts toward binding WT sACE2$_2$ were observed (fig. S6). Two S mutants were investigated further in sACE2$_2$ titration experiments, N501W and N501Y, which both retained high receptor binding and displayed small shifts toward WT sACE2$_2$ in the competition experiment. N501 of S is located in the 498-506 loop, and its substitution to large aromatic side chains might alter the loop conformation to cause steric strain with nearby ACE2 mutation N330Y in sACE2$_2$.v2.4. After titrating the concentrations of 8his-tagged sACE2$_2$(WT) and sACE2$_2$.v2.4 and measuring bound protein to S-expressing cells by flow cytometry, it was found that S-N501W and S-N501Y do show enhanced specificity for WT sACE2$_2$, but the effect is small and sACE2$_2$.v2.4 remains to be the stronger binder (Fig. 5C).

Dimeric sACE2$_2$ binds avidly to S protein on a membrane surface; avid interactions are also observed between sACE2$_2$ and spikes on authentic SARS-CoV-2 in infection assays (*27*). We used BLI kinetics measurements, in which immobilized sACE2$_2$-IgG1 interacts with monomeric RBD, to determine how the observed changes in avid sACE2$_2$ binding to S-expressing cells translate to changes in affinity. Both N501W and N501Y mutants of SARS-CoV-2 RBD displayed increased affinity for WT ACE2 and engineered ACE2.v2.4, with larger affinity gains in favor of the WT receptor (Table 1). This aligns with the flow cytometry data indicating a small shift in specificity toward WT ACE2, but not enough to escape the engineered decoy. By comparison, multiple independent escape mutations are

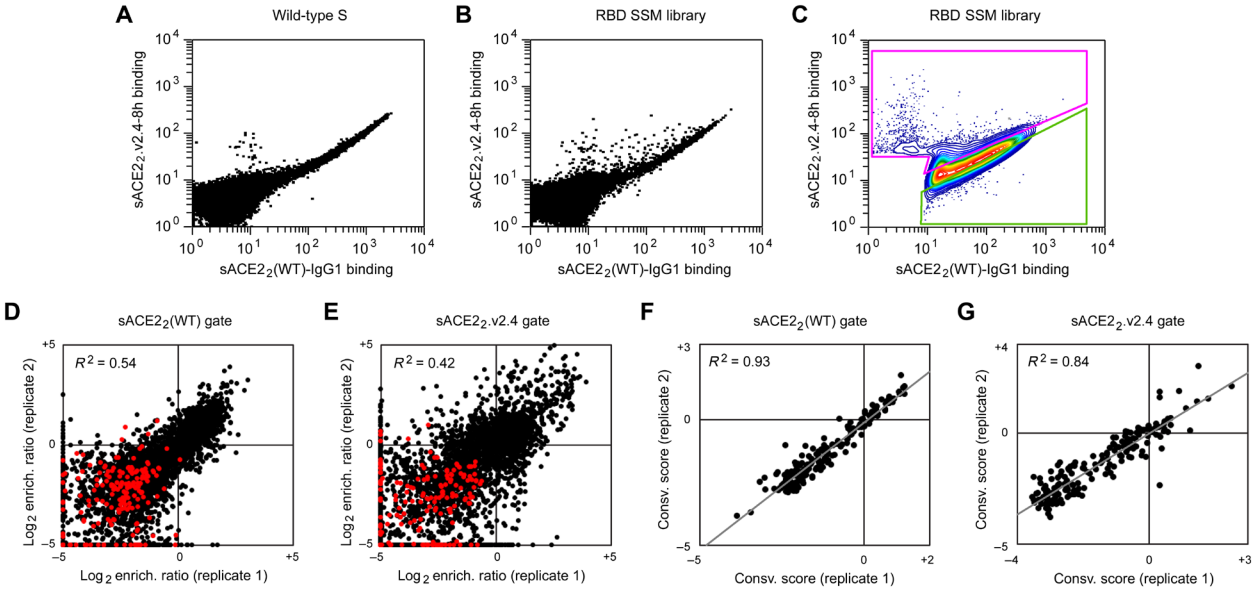

Fig. 4. A competition-based selection to identify RBD mutations within S of SARS-CoV-2 that preferentially bind WT or engineered ACE2 receptors. (**A**) Expi293F cells were transfected with WT myc-S and incubated with competing sACE2$_2$(WT)-IgG1 (25 nM) and sACE2$_2$.v2.4-8h (20 nM). Bound protein was detected by flow cytometry after immunostaining for the respective epitope tags. (**B**) As in (A), except cells were transfected with the RBD SSM library. A population of cells expressing S variants with increased specificity toward sACE2$_2$.v2.4 is apparent (cells shifted to the upper left of the main population). (**C**) Gates used for FACS of cells expressing the RBD SSM library. After excluding cells without bound protein, the top 20% of cells for bound sACE2$_2$.v2.4-8h (magenta gate) and for bound sACE2$_2$(WT)-IgG1 (green gate) were collected. (**D** and **E**) Agreement between log$_2$ enrichment ratios from two independent FACS selections for cells expressing S variants with increased specificity for (D) sACE2$_2$(WT) or (E) sACE2$_2$.v2.4. R^2 values are calculated for nonsynonymous mutations (black). Nonsense mutations are red. (**F** and **G**) Conservation scores are calculated from the mean of the log$_2$ enrichment ratios for all nonsynonymous substitutions at a given residue position. Correlation plots show agreement between conservation scores for two independent selections for cells within the (D) sACE2$_2$(WT)- or (E) sACE2$_2$.v2.4-specific gates.

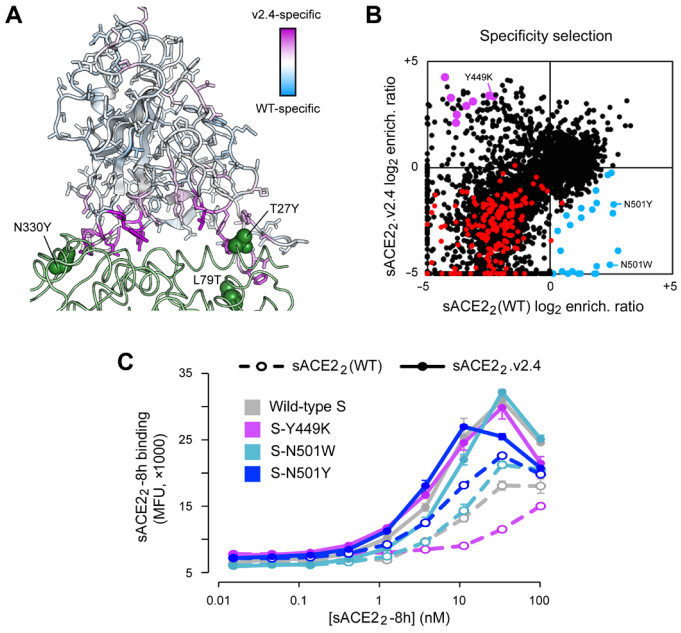

Fig. 5. Mutations within the RBD that confer specificity toward WT ACE2 are rare. (**A**) The SARS-CoV-2 RBD is colored by specificity score [the difference between the conservation scores for cells collected in the $sACE2_2$(WT)- and $sACE2_2$.v2.4-specific gates]. Residues that are hotspots for mutations with increased specificity toward $sACE2_2$(WT) are blue or toward $sACE2_2$.v2.4 are purple. The contacting surface of ACE2 is shown as a green ribbon, with sites of mutations in $sACE2_2$.v2.4 labeled and shown as green spheres. (**B**) Log_2 enrichment ratios for mutations in S expressed by cell populations collected in the $sACE2_2$(WT)-specific (*x* axis) and $sACE2_2$.v2.4-specific (*y* axis) gates. Data are the mean from two independent sorting experiments. S mutants in blue were predicted to have increased specificity for $sACE2_2$(WT) and were tested by targeted mutagenesis in fig. S6. S mutants in purple were predicted to have increased specificity for $sACE2_2$.v2.4 and were tested by targeted mutagenesis in fig. S7. Other nonsynonymous mutations are black. Nonsense mutations are red. (**C**) WT myc-S (gray) and three variants, Y449K (purple), N501W (light blue), and N501Y (dark blue), were expressed in Expi293F cells and tested by flow cytometry for binding to $sACE2_2$(WT)-8h (dashed lines) or $sACE2_2$.v2.4-8h (solid lines). MFU, mean fluorescence units.

readily found in S of SARS-CoV-2 that diminish the efficacy of monoclonal antibodies by many orders of magnitude (*20*, *21*).

Last, eight representative mutations to S predicted from the deep mutational scan to increase specificity toward $sACE2_2$.v2.4 (purple data points in Fig. 5B) were cloned, and seven were found to have large shifts toward preferential $sACE2_2$.v2.4 binding in the competition assay (fig. S7). These S mutations were Y449K/Q/S, L455G/R/Y, and G504K. The basis for why the mutations increase specificity toward engineered $sACE2_2$.v2.4 is ambiguous, since RBD residues Y449, L455, and G504 are not in direct contact with engineered sites of the receptor. BLI kinetics between immobilized $sACE2_2$-IgG1 and monomeric RBD as the analyte showed reduced affinity of a representative mutant, RBD-Y449K, to both WT and engineered $sACE2_2$ (Table 1). However, affinity changes in the picomolar range for $sACE2_2$.v2.4 are hidden during avid binding to full-length S-Y449K at the cell surface, whereas avid binding of WT $sACE2_2$ to S-Y449K (with affinity measured by BLI in the moderate nanomolar range) is substantially reduced. This finding might explain why the competition selection found many mutations that shift specificity toward engineered $sACE2_2$.v2.4, as mutations causing small decreases in affinity may have larger effects on avid binding of the weaker-bound WT receptor.

Overall, validation by targeted mutagenesis confirms that the selection can successfully find mutations in S with altered specificity. The inability to find mutations in the RBD that impart high specificity for the WT receptor means that such mutations are rare or may not even exist, at least within the RBD where direct physical contacts with receptors occur. We cannot exclude mutations elsewhere having long-range conformational effects. Engineered, soluble decoy receptors therefore live up to their promise as broad therapeutic candidates against which a virus cannot easily escape.

DISCUSSION

The allure of soluble decoy receptors is that the virus cannot easily mutate to escape neutralization. Mutations that reduce affinity of the soluble decoy will likely also decrease affinity for the WT receptor on host cells, thereby coming at the cost of diminished infectivity and virulence. However, this hypothesis has not been rigorously tested, and since engineered decoy receptors differ from their WT counterparts, even if by just a small number of mutations, it is possible that a virus may evolve to discriminate between the two. Here, we show that an engineered decoy receptor for SARS-CoV-2 broadly binds with low-nanomolar K_D to the spikes of SARS-associated betacoronaviruses that use ACE2 for entry, despite high sequence diversity within the ACE2-binding site. Mutations in S of SARS-CoV-2 that confer high specificity for WT ACE2 were not found in a comprehensive screen of all substitutions within the RBD. The engineered decoy receptor is therefore broad against zoonotic ACE2-utilizing coronaviruses that may spill over from animal reservoirs in the future and against variants of SARS-CoV-2 that may arise as the current COVID-19 pandemic rages on. These findings are highly consistent with research of a high-affinity decoy receptor engineered for a different pathogen, HIV. An IgG1 Fc–fused soluble decoy based on HIV receptors, called eCD4-Ig, broadly neutralizes HIV-1, HIV-2, and related simian viruses, with single mutations in the HIV spike protein unable to achieve full escape (*47*, *48*). Together with the results reported here, these studies collectively demonstrate that engineered decoy receptors can achieve exceptional breadth against virus sequence variants. We argue that it is unlikely that decoy receptors will need to be combined in cocktail formulations, as is required for many monoclonal antibodies and possibly designed miniprotein binders to prevent the rapid emergence of resistance (*20*, *49*), facilitating manufacture and distribution. Our findings give insight into how a potential therapeutic can achieve breadth with a low chance of virus resistance for a family of highly infectious and deadly viruses.

MATERIALS AND METHODS

Plasmids

Residue numbers for constructs begin from the start methionine as a.a. 1. The cloning of human codon-optimized, mature S from SARS-CoV-2 (GenBank accession number YP_009724390.1; a.a. V16 to T1273) into the Nhe I–Xho I sites of pCEP4 (Invitrogen) with an N-terminal, extracellular c-myc tag is described elsewhere (*27*). sACE2 (a.a. 1 to 732 encoding a dimer; WT or engineered variant $sACE2_2$.v2.4) fused to an 8his purification tag or to human IgG1 Fc (a.a. D221-K447; nG1m1 isoallotype; GenBank KY432415.1) and cloned into the Nhe I–Xho I sites of pcDNA3.1(+) (Invitrogen) is

also previously described (*27*). The RBDs of SARS-CoV-1 (Urbani isolate; GenBank AAP13441.1; a.a. T320 to D518), SARS-CoV-2 (YP_009724390; a.a. T333 to K529), LYRa11 (AHX37558.1; a.a. T324 to D522), Rs7327 (ATO98218.1; a.a. T321 to D519), Rs4231 (ATO98157.1; a.a. T320 to D518), Rs4084 (ATO98132.1; a.a. T321-D519), and RsSHC014 (AGZ48806.1; a.a. T321-D519) were cloned with N-terminal influenza HA leader peptides (sequence MKTIIALSYIFCLVFA) and C-terminal 8his tags (sequence GSGHHHHHHHH) into the Nhe I–Xho I sites of pcDNA3.1(+). These plasmids are deposited with Addgene under accession numbers 145145, 164845, and 161821-161826. Mutations were made by overlap extension polymerase chain reaction (PCR) and verified by Sanger sequencing.

Tissue culture

Expi293F cells (Thermo Fisher Scientific) were grown in Expi293 Expression Medium (Thermo Fisher Scientific) at 125 rpm, 8% CO_2, 37°C.

Recombinant protein production

Plasmids (500 ng of DNA/ml culture) and polyethylenimine (MW 25,000; Polysciences; 3 μg/ml culture) were mixed with OptiMEM (Gibco; 100 μl/ml culture), incubated 20 min at room temperature and added to Expi293F cells at a density of 2×10^6/ml. Transfection Enhancers (Thermo Fisher Scientific) were added 18 to 23 hours after transfection. Culture supernatant was harvested 4 to 6 days later by two centrifugation steps (800*g* for 10 min to remove cells and 20,000*g* for 20 min to remove debris). IgG1 Fc–fused and 8his-tagged proteins were subsequently purified as previously described (*27*) using KANEKA KanCapA 3G Affinity (Pall) and HisPur Ni-NTA (Thermo Fisher Scientific) resins, respectively. Eluted proteins from affinity chromatography were then separated on a Superdex 200 Increase 10/300 GL column (GE Healthcare Life Sciences) equilibrated with Dulbecco's phosphate-buffered saline (PBS). Proteins from peak fractions were concentrated using centrifugal ultrafiltration devices (Millipore) to final concentrations of ~1 mg/ml (RBD-8h proteins), ~10 mg/ml ($sACE2_2$-8h proteins), and ~50 mg/ml ($sACE2_2$-IgG1 proteins). Concentrations were determined by absorbance at 280 nm using calculated extinction coefficients. Reported concentrations for $sACE2_2$ are based on monomeric subunits. Aliquots were snap frozen in liquid N_2 and stored at −80°C.

Biolayer interferometry

BLI kinetics were collected on an Octet RED96a and analyzed with a 1:1 binding model (global fit) using instrument software (Molecular Devices). IgG1 Fc–fused $sACE2_2$ (WT or engineered variant $sACE2_2$.v2.4) was immobilized at 100 nM for 10 min to anti-human IgG Fc biosensors (Molecular Devices). The assay buffer was 10 mM Hepes (pH 7.6), 150 mM NaCl, 3 mM EDTA, 0.05% polysorbate 20, and 0.5% nonfat dry milk (Bio-Rad). Loaded sensors were equilibrated for 30 s in buffer, then dipped in RBD-8h solutions for 60 s to measure association, and transferred back to buffer to measure dissociation over 300 s.

Library construction, FACS, and Illumina sequencing analysis

Using plasmid pCEP4-myc-S encoding tagged, full-length S of SARS-CoV-2, saturation mutagenesis was focused to residues C336 to L517 forming the RBD. Degenerate NNK codons were introduced at all RBD positions using overlap extension PCR as previously described (*50*). Transient transfection conditions were used that typically provide no more than a single coding variant per cell (*36*, *37*). Expi293F cells at 2×10^6/ml were transfected with a mixture of 1 ng of coding plasmid (i.e., library DNA) with 1.5 μg of pCEP4-ΔCMV carrier plasmid [described in (*37*)]. The medium was replaced 2 hours after transfection, and cells were collected 24 hours after transfection for FACS. Cells were washed with ice-cold PBS supplemented with 0.2% bovine serum albumin (PBS-BSA).

For investigations of binding to WT $sACE2_2$, the cells expressing the S library were resuspended in 2.5 nM $sACE2_2$(WT)-8h and incubated 30 min on ice. Cells were washed twice with PBS-BSA and then costained for 20 min with anti-myc Alexa Fluor 647 (clone 9B11, 1/250 dilution; Cell Signaling Technology) and anti–HIS–fluorescein isothiocyanate (FITC) (chicken polyclonal, 1/100 dilution; Immunology Consultants Laboratory). Cells were again washed twice before sorting on a BD FACSAria II at the Roy J. Carver Biotechnology Center. Dead cells, doublets, and debris were excluded by first gating on the main population by forward/side scattering and then excluding 4′,6-diamidino-2-phenylindole–positive cells. From the myc-S–positive (Alexa Fluor 647) population, the 20% of cells with the highest and 20% of cells with the lowest anti–HIS-FITC fluorescence for bound $sACE2_2$(WT)-8h were collected (Fig. 2C). Collection tubes were coated overnight with fetal bovine serum before sorting and contained an Expi293 Expression Medium. Fluorescent signals decreased over time during FACS, and therefore, transfected cultures were prepared on three separate occasions for a combined total of 8-hour sort time. The total numbers of collected cells were 57,000 and 72,700 for the ACE2-high and ACE2-low gates, respectively. Collected cells were centrifuged (500*g*, 300 s), and pellets were frozen at −80°C. Samples from the independent sorts were pooled during extraction of total RNA.

The competition selection was performed similarly, with the exception that cells expressing the S library were incubated for 30 min in a mixture of 20 nM $sACE2_2$.v2.4-8h and 25 nM $sACE2_2$(WT)-IgG1. After washing twice, bound proteins were stained for 30 min with anti-human IgG-allophycocyaninc (APC) (clone HP6017, 1/250 dilution; BioLegend) and anti–HIS-FITC (chicken polyclonal, 1/100 dilution; Immunology Consultants Laboratory). Cells were washed twice and sorted. After gating for the main population of viable cells as described above, the 20% of cells with the highest FITC relative to APC and highest APC relative to FITC signals were collected (Fig. 4C). The total numbers of collected cells were 53,950 [replicate 1: $sACE2_2$(WT)-specific gate], 42,860 (replicate 1: $sACE2_2$.v2.4-specific gate), 41,420 [replicate 2: $sACE2_2$(WT)-specific gate], and 34,730 (replicate 2: $sACE2_2$.v2.4-specific gate).

Total RNA was extracted from the collected cells using a GeneJET RNA purification kit (Thermo Fisher Scientific). First-strand complementary DNA (cDNA) was synthesized with Accuscript (Agilent) primed with a gene-specific oligonucleotide. The region of S scanned by saturation mutagenesis was PCR amplified as three overlapping fragments that together span the full RBD sequence. Following a second round of PCR, primers added adapters for annealing to the Illumina flow cell and sequencing primers, together with barcodes for experiment identification. The PCR products were sequenced on an Illumina NovaSeq 6000 using a 2 × 250 nucleotide paired-end protocol. Data were analyzed using Enrich (*38*), where the frequencies of S variants in the transcripts of the sorted populations were compared to their frequencies in the naïve plasmid library. Log_2 enrichment ratios for all the individual mutations were calculated and normalized

by subtracting the $\log_2$ enrichment ratio for the WT sequence across the same PCR-amplified fragment. Conservation scores at residue positions were calculated by averaging the $\log_2$ enrichment ratios for all nonsynonymous mutations at the residue.

Flow cytometry analysis of SARS-CoV-2 S mutants

Expi293F cells at 2.0×10^6 cells/ml were transfected with plasmid DNA (300 ng/ml of culture for measuring myc-S surface expression and $sACE2_2$ competition binding and 500 ng/ml for titration experiments) encoding myc-S variants using Expifectamine (Thermo Fisher Scientific) according to the manufacturer's directions. At 24 hours after transfection, cells were washed with PBS-BSA. To detect surface-expressed myc-S, cells were incubated with anti-myc Alexa Fluor 647 (clone 9B11, 1/250 dilution; Cell Signaling Technology) on a rocker at 4°C for 30 min. To measure competitive binding of WT and engineered receptors, cells were instead incubated with 25 nM $sACE2_2$(WT)-IgG1 and 20 nM $sACE2_2$.v2.4-8h for 30 min at 4°C, washed twice, and stained with anti-human IgG-APC (clone HP6017, 1/250 dilution; BioLegend) and anti–HIS-FITC (chicken polyclonal, 1/100 dilution; Immunology Consultants Laboratory) secondary antibodies for 20 min at 4°C. Last, in titration experiments, transfected cells were incubated for 30 min at 4°C with one-third serial dilutions of sACE22(WT)-8h or sACE22.v2.4-8h, followed by two washes and a 30-min incubation with anti-myc Alexa Fluor 647 (clone 9B11, 1/250 dilution) and anti–HIS-FITC (chicken polyclonal, 1/100 dilution). For all experiments, cells were washed twice before analysis on an Accuri C6 Flow Cytometer (BD Biosciences), and data were processed with FCS Express (De Novo Software). Quantification of myc-S surface expression is detailed in fig. S5.

Reagent and data availability

Plasmids for RBD protein expression are deposited with Addgene (numbers 145145, 164845, and 161821-161826). Illumina sequencing data are deposited in the National Center for Biotechnology Information's Gene Expression Omnibus under series accession number GSE159372.

SUPPLEMENTARY MATERIALS

Supplementary material for this article is available at http://advances.sciencemag.org/cgi/content/full/7/8/eabf1738/DC1

View/request a protocol for this paper from *Bio-protocol*.

REFERENCES AND NOTES

1. P. Zhou, X.-L. Yang, X.-G. Wang, B. Hu, L. Zhang, W. Zhang, H.-R. Si, Y. Zhu, B. Li, C.-L. Huang, H.-D. Chen, J. Chen, Y. Luo, H. Guo, R.-D. Jiang, M.-Q. Liu, Y. Chen, X.-R. Shen, X. Wang, X.-S. Zheng, K. Zhao, Q.-J. Chen, F. Deng, L.-L. Liu, B. Yan, F.-X. Zhan, Y.-Y. Wang, G.-F. Xiao, Z.-L. Shi, A pneumonia outbreak associated with a new coronavirus of probable bat origin. *Nature* **579**, 270–273 (2020).
2. A. C. Walls, Y.-J. Park, M. A. Tortorici, A. Wall, A. T. McGuire, D. Veesler, Structure, function, and antigenicity of the SARS-CoV-2 spike glycoprotein. *Cell* **181**, 281–292.e6 (2020).
3. Y. Wan, J. Shang, R. Graham, R. S. Baric, F. Li, Receptor recognition by novel coronavirus from Wuhan: An analysis based on decade-long structural studies of SARS coronavirus. *J. Virol.* **94**, e00127-20 (2020).
4. D. Wrapp, N. Wang, K. S. Corbett, J. A. Goldsmith, C.-L. Hsieh, O. Abiona, B. S. Graham, J. S. McLellan, Cryo-EM structure of the 2019-nCoV spike in the prefusion conformation. *Science* **367**, 1260–1263 (2020).
5. M. Hoffmann, H. Kleine-Weber, S. Schroeder, N. Krüger, T. Herrler, S. Erichsen, T. S. Schiergens, G. Herrler, N.-H. Wu, A. Nitsche, M. A. Müller, C. Drosten, S. Pöhlmann, SARS-CoV-2 cell entry depends on ACE2 and TMPRSS2 and is blocked by a clinically proven protease inhibitor. *Cell* **181**, 271–280.e8 (2020).
6. W. Li, M. J. Moore, N. Vasilieva, J. Sui, S. K. Wong, M. A. Berne, M. Somasundaran, J. L. Sullivan, K. Luzuriaga, T. C. Greenough, H. Choe, M. Farzan, Angiotensin-converting enzyme 2 is a functional receptor for the SARS coronavirus. *Nature* **426**, 450–454 (2003).
7. M. Letko, A. Marzi, V. Munster, Functional assessment of cell entry and receptor usage for SARS-CoV-2 and other lineage B betacoronaviruses. *Nat. Microbiol.* **5**, 562–569 (2020).
8. L. Samavati, B. D. Uhal, ACE2, much more than just a receptor for SARS-COV-2. *Front. Cell. Infect. Microbiol.* **10**, 317 (2020).
9. F. Jiang, J. Yang, Y. Zhang, M. Dong, S. Wang, Q. Zhang, F. F. Liu, K. Zhang, C. Zhang, Angiotensin-converting enzyme 2 and angiotensin 1–7: Novel therapeutic targets. *Nat. Rev. Cardiol.* **11**, 413–426 (2014).
10. L. Zhang, C. B. Jackson, H. Mou, A. Ojha, E. S. Rangarajan, T. Izard, M. Farzan, H. Choe, The D614G mutation in the SARS-CoV-2 spike protein reduces S1 shedding and increases infectivity. *bioRxiv* 2020.06.12.148726 , (2020).
11. B. Korber, W. M. Fischer, S. Gnanakaran, H. Yoon, J. Theiler, W. Abfalterer, N. Hengartner, E. E. Giorgi, T. Bhattacharya, B. Foley, K. M. Hastie, M. D. Parker, D. G. Partridge, C. M. Evans, T. M. Freeman, T. I. de Silva, Tracking changes in SARS-CoV-2 Spike: Evidence that D614G increases infectivity of the COVID-19 virus. *Cell* **182**, 812–827.e19 (2020).
12. V. Borges, J. Isidro, H. Cortes-Martins, S. Duarte, L. Vieira, R. Leite, I. Gordo, C. P. Caetano, B. Nunes, R. Sá, A. Oliveira, R. Guiomar, J. P. Gomes; Portuguese Network for SARS-CoV-2 Genomics, On the track of the D839Y mutation in the SARS-CoV-2 spike fusion peptide: Emergence and geotemporal spread of a highly prevalent variant in Portugal. *medRxiv* 2020.08.10.20171884 , (2020).
13. D. S. Candido, I. M. Claro, J. G. de Jesus, W. M. Souza, F. R. R. Moreira, S. Dellicour, T. A. Mellan, L. du Plessis, R. H. M. Pereira, F. C. S. Sales, E. R. Manuli, J. Thézé, L. Almeida, M. T. Menezes, C. M. Voloch, M. J. Fumagalli, T. M. Coletti, C. A. M. da Silva, M. S. Ramundo, M. R. Amorim, H. H. Hoeltgebaum, S. Mishra, M. S. Gill, L. M. Carvalho, L. F. Buss, C. A. Prete Jr., J. Ashworth, H. I. Nakaya, P. S. Peixoto, O. J. Brady, S. M. Nicholls, A. Tanuri, Á. D. Rossi, C. K. V. Braga, A. L. Gerber, A. P. de C. Guimarães, N. Gaburo Jr., C. S. Alencar, A. C. S. Ferreira, C. X. Lima, J. E. Levi, C. Granato, G. M. Ferreira, R. S. Francisco Jr., F. Granja, M. T. Garcia, M. L. Moretti, M. W. Perroud Jr., T. M. P. P. Castiñeiras, C. S. Lazari, S. C. Hill, A. A. de Souza Santos, C. L. Simeoni, J. Forato, A. C. Sposito, A. Z. Schreiber, M. N. N. Santos, C. Z. de Sá, R. P. Souza, L. C. Resende-Moreira, M. M. Teixeira, J. Hubner, P. A. F. Leme, R. G. Moreira, M. L. Nogueira; Brazil-UK Centre for Arbovirus Discovery, Diagnosis, Genomics and Epidemiology (CADDE) Genomic Network, N. M. Ferguson, S. F. Costa, J. L. Proenca-Modena, A. T. R. Vasconcelos, S. Bhatt, P. Lemey, C.-H. Wu, A. Rambaut, N. J. Loman, R. S. Aguiar, O. G. Pybus, E. C. Sabino, N. R. Faria, Evolution and epidemic spread of SARS-CoV-2 in Brazil. *Science* **369**, 1255–1260 (2020).
14. B. B. Oude Munnink, R. S. Sikkema, D. F. Nieuwenhuijse, R. J. Molenaar, E. Munger, R. Molenkamp, A. van der Spek, P. Tolsma, A. Rietveld, M. Brouwer, N. Bouwmeester-Vincken, F. Harders, R. Hakze-van der Honing, M. C. A. Wegdam-Blans, R. J. Bouwstra, C. GeurtsvanKessel, A. A. van der Eijk, F. C. Velkers, L. A. M. Smit, A. Stegeman, W. H. M. van der Poel, M. P. G. Koopmans, Transmission of SARS-CoV-2 on mink farms between humans and mink and back to humans. *Science* **371**, 172–177 (2021).
15. S. Su, G. Wong, W. Shi, J. Liu, A. C. K. Lai, J. Zhou, W. Liu, Y. Bi, G. F. Gao, Epidemiology, genetic recombination, and pathogenesis of coronaviruses. *Trends Microbiol.* **24**, 490–502 (2016).
16. M. F. Boni, P. Lemey, X. Jiang, T. T.-Y. Lam, B. W. Perry, T. A. Castoe, A. Rambaut, D. L. Robertson, Evolutionary origins of the SARS-CoV-2 sarbecovirus lineage responsible for the COVID-19 pandemic. *Nat. Microbiol.* **5**, 1408–1417 (2020).
17. J. S. M. Sabir, T. T.-Y. Lam, M. M. M. Ahmed, L. Li, Y. Shen, S. E. M. Abo-Aba, M. I. Qureshi, M. Abu-Zeid, Y. Zhang, M. A. Khiyami, N. S. Alharbi, N. H. Hajrah, M. J. Sabir, M. H. Z. Mutwakil, S. A. Kabli, F. A. S. Alsulaimany, A. Y. Obaid, B. Zhou, D. K. Smith, E. C. Holmes, H. Zhu, Y. Guan, Co-circulation of three camel coronavirus species and recombination of MERS-CoVs in Saudi Arabia. *Science* **351**, 81–84 (2016).
18. D. VanInsberghe, A. Neish, A. C. Lowen, K. Koelle, Identification of SARS-CoV-2 recombinant genomes. *bioRxiv* 2020.08.05.238386 , (2020).
19. X. Li, E. E. Giorgi, M. H. Marichannegowda, B. Foley, C. Xiao, X.-P. Kong, Y. Chen, S. Gnanakaran, B. Korber, F. Gao, Emergence of SARS-CoV-2 through recombination and strong purifying selection. *Sci. Adv.* **6**, eabb9153 (2020).
20. A. Baum, B. O. Fulton, E. Wloga, R. Copin, K. E. Pascal, V. Russo, S. Giordano, K. Lanza, N. Negron, M. Ni, Y. Wei, G. S. Atwal, A. J. Murphy, N. Stahl, G. D. Yancopoulos, C. A. Kyratsous, Antibody cocktail to SARS-CoV-2 spike protein prevents rapid mutational escape seen with individual antibodies. *Science* **369**, 1014–1018 (2020).
21. A. J. Greaney, T. N. Starr, P. Gilchuk, S. J. Zost, E. Binshtein, A. N. Loes, S. K. Hilton, J. Huddleston, R. Eguia, K. H. D. Crawford, A. S. Dingens, R. S. Nargi, R. E. Sutton, N. Suryadevara, P. W. Rothlauf, Z. Liu, S. P. J. Whelan, R. H. Carnahan, J. E. Crowe Jr., J. D. Bloom, Complete mapping of mutations to the SARS-CoV-2 spike receptor-binding domain that escape antibody recognition. *Cell Host Microbe* S1931-3128(20)30624-7 , (2020).
22. M. A. Tortorici, M. Beltramello, F. A. Lempp, D. Pinto, H. V. Dang, L. E. Rosen, M. M. Callum, J. Bowen, A. Minola, S. Jaconi, F. Zatta, A. De Marco, B. Guarino, S. Bianchi, E. J. Lauron, H. Tucker, J. Zhou, A. Peter, C. Havenar-Daughton, J. A. Wojcechowskyj, J. B. Case, R. E. Chen, H. Kaiser, M. Montiel-Ruiz, M. Meury, N. Czudnochowski, R. Spreafico, J. Dillen, C. Ng, N. Sprugasci, K. Culap, F. Benigni, R. Abdelnabi, S.-Y. C. Foo, M. A. Schmid, E. Cameroni, A. Riva, A. Gabrieli, M. Galli, M. S. Pizzuto, J. Neyts, M. S. Diamond,

H. W. Virgin, G. Snell, D. Corti, K. Fink, D. Veesler, Ultrapotent human antibodies protect against SARS-CoV-2 challenge via multiple mechanisms. *Science* **370**, 950–957 (2020).
23. D. Pinto, Y.-J. Park, M. Beltramello, A. C. Walls, M. A. Tortorici, S. Bianchi, S. Jaconi, K. Culap, F. Zatta, A. De Marco, A. Peter, B. Guarino, R. Spreafico, E. Cameroni, J. B. Case, R. E. Chen, C. Havenar-Daughton, G. Snell, A. Telenti, H. W. Virgin, A. Lanzavecchia, M. S. Diamond, K. Fink, D. Veesler, D. Corti, Cross-neutralization of SARS-CoV-2 by a human monoclonal SARS-CoV antibody. *Nature* **583**, 290–295 (2020).
24. H. Hofmann, M. Geier, A. Marzi, M. Krumbiegel, M. Peipp, G. H. Fey, T. Gramberg, S. Pöhlmann, Susceptibility to SARS coronavirus S protein-driven infection correlates with expression of angiotensin converting enzyme 2 and infection can be blocked by soluble receptor. *Biochem. Biophys. Res. Commun.* **319**, 1216–1221 (2004).
25. C. Lei, K. Qian, T. Li, S. Zhang, W. Fu, M. Ding, S. Hu, Neutralization of SARS-CoV-2 spike pseudotyped virus by recombinant ACE2-Ig. *Nat. Commun.* **11**, 2070 (2020).
26. V. Monteil, H. Kwon, P. Prado, A. Hagelkrüys, R. A. Wimmer, M. Stahl, A. Leopoldi, E. Garreta, C. Hurtado del Pozo, F. Prosper, J. P. Romero, G. Wirnsberger, H. Zhang, A. S. Slutsky, R. Conder, N. Montserrat, A. Mirazimi, J. M. Penninger, Inhibition of SARS-CoV-2 infections in engineered human tissues using clinical-grade soluble human ACE2. *Cell* **181**, 905–913.e7 (2020).
27. K. K. Chan, D. Dorosky, P. Sharma, S. A. Abbasi, J. M. Dye, D. M. Kranz, A. S. Herbert, E. Procko, Engineering human ACE2 to optimize binding to the spike protein of SARS coronavirus 2. *Science* **369**, 1261–1265 (2020).
28. A. Zoufaly, M. Poglitsch, J. H. Aberle, W. Hoepler, T. Seitz, M. Traugott, A. Grieb, E. Pawelka, H. Laferl, C. Wenisch, S. Neuhold, D. Haider, K. Stiasny, A. Bergthaler, E. Puchhammer-Stoeckl, A. Mirazimi, N. Montserrat, H. Zhang, A. S. Slutsky, J. M. Penninger, Human recombinant soluble ACE2 in severe COVID-19. *Lancet Respir. Med.* **8**, 1154–1158 (2020).
29. A. Glasgow, J. Glasgow, D. Limonta, P. Solomon, I. Lui, Y. Zhang, M. A. Nix, N. J. Rettko, S. Zha, R. Yamin, K. Kao, O. S. Rosenberg, J. V. Ravetch, A. P. Wiita, K. K. Leung, S. A. Lim, X. X. Zhou, T. C. Hobman, T. Kortemme, J. A. Wells, Engineered ACE2 receptor traps potently neutralize SARS-CoV-2. *Proc. Natl. Acad. Sci. U.S.A.* **117**, 28046–28055 (2020).
30. Y. Higuchi, T. Suzuki, T. Arimori, N. Ikemura, Y. Kirita, E. Ohgitani, O. Mazda, D. Motooka, S. Nakamura, Y. Matsuura, S. Matoba, T. Okamoto, J. Takagi, A. Hoshino, High affinity modified ACE2 receptors prevent SARS-CoV-2 infection. *bioRxiv* 2020.09.16.299891, (2020).
31. H. K. Frank, D. Enard, S. D. Boyd, Exceptional diversity and selection pressure on SARS-CoV and SARS-CoV-2 host receptor in bats compared to other mammals. *bioRxiv* 2020.04.20.051656, (2020).
32. J. Shang, G. Ye, K. Shi, Y. Wan, C. Luo, H. Aihara, Q. Geng, A. Auerbach, F. Li, Structural basis of receptor recognition by SARS-CoV-2. *Nature* **581**, 221–224 (2020).
33. R. N. Kirchdoerfer, N. Wang, J. Pallesen, D. Wrapp, H. L. Turner, C. A. Cottrell, K. S. Corbett, B. S. Graham, J. S. McLellan, A. B. Ward, Stabilized coronavirus spikes are resistant to conformational changes induced by receptor recognition or proteolysis. *Sci. Rep.* **8**, 15701 (2018).
34. W. Li, C. Zhang, J. Sui, J. H. Kuhn, M. J. Moore, S. Luo, S.-K. Wong, I.-C. Huang, K. Xu, N. Vasilieva, A. Murakami, Y. He, W. A. Marasco, Y. Guan, H. Choe, M. Farzan, Receptor and viral determinants of SARS-coronavirus adaptation to human ACE2. *EMBO J.* **24**, 1634–1643 (2005).
35. D. M. Fowler, S. Fields, Deep mutational scanning: A new style of protein science. *Nat. Methods* **11**, 801–807 (2014).
36. J. D. Heredia, J. Park, R. J. Brubaker, S. K. Szymanski, K. S. Gill, E. Procko, Mapping interaction sites on human chemokine receptors by deep mutational scanning. *J. Immunol.* **200**, 3825–3839 (2018).
37. J. Park, B. Selvam, K. Sanematsu, N. Shigemura, D. Shukla, E. Procko, Structural architecture of a dimeric class C GPCR based on co-trafficking of sweet taste receptor subunits. *J. Biol. Chem.* **294**, 4759–4774 (2019).
38. D. M. Fowler, C. L. Araya, W. Gerard, S. Fields, Enrich: Software for analysis of protein function by enrichment and depletion of variants. *Bioinformatics* **27**, 3430–3431 (2011).
39. K. Wu, G. Peng, M. Wilken, R. J. Geraghty, F. Li, Mechanisms of host receptor adaptation by severe acute respiratory syndrome coronavirus. *J. Biol. Chem.* **287**, 8904–8911 (2012).
40. T. N. Starr, A. J. Greaney, S. K. Hilton, D. Ellis, K. H. D. Crawford, A. S. Dingens, M. J. Navarro, J. E. Bowen, M. A. Tortorici, A. C. Walls, N. P. King, D. Veesler, J. D. Bloom, Deep mutational scanning of SARS-CoV-2 receptor binding domain reveals constraints on folding and ACE2 binding. *Cell* **182**, 1295–1310.e20 (2020).
41. E. Volz, S. Mishra, M. Chand, J. C. Barrett, R. Johnson, L. Geidelberg, W. R. Hinsley, D. J. Laydon, G. Dabrera, Á. O'Toole, R. Amato, M. Ragonnet-Cronin, I. Harrison, B. Jackson, C. V. Ariani, O. Boyd, N. J. Loman, J. T. McCrone, S. Gonçalves, D. Jorgensen, R. Myers, V. Hill, D. K. Jackson, K. Gaythorpe, N. Groves, J. Sillitoe, D. P. Kwiatkowski; The COVID-19 Genomics UK (COG-UK) consortium, S. Flaxman, O. Ratmann, S. Bhatt, S. Hopkins, A. Gandy, A. Rambaut, N. M. Ferguson, Transmission of SARS-CoV-2 Lineage B.1.1.7 in England: Insights from linking epidemiological and genetic data. *medRxiv* 2020.12.30.20249034 (2020).
42. T. W. Linsky, R. Vergara, N. Codina, J. W. Nelson, M. J. Walker, W. Su, C. O. Barnes, T.-Y. Hsiang, K. Esser-Nobis, K. Yu, Z. B. Reneer, Y. J. Hou, T. Priya, M. Mitsumoto, A. Pong, U. Y. Lau, M. L. Mason, J. Chen, A. Chen, T. Berrocal, H. Peng, N. S. Clairmont, J. Castellanos, Y.-R. Lin, A. Josephson-Day, R. S. Baric, D. H. Fuller, C. D. Walkey, T. M. Ross, R. Swanson, P. J. Bjorkman, M. Gale Jr., L. M. Blancas-Mejia, H.-L. Yen, D.-A. Silva, De novo design of potent and resilient hACE2 decoys to neutralize SARS-CoV-2. *Science* **370**, 1208–1214 (2020).
43. Y. Cai, J. Zhang, T. Xiao, H. Peng, S. M. Sterling, R. M. Walsh Jr., S. Rawson, S. Rits-Volloch, B. Chen, Distinct conformational states of SARS-CoV-2 spike protein. *Science* **369**, 1586–1592 (2020).
44. H. Yao, Y. Song, Y. Chen, N. Wu, J. Xu, C. Sun, J. Zhang, T. Weng, Z. Zhang, Z. Wu, L. Cheng, D. Shi, X. Lu, J. Lei, M. Crispin, Y. Shi, L. Li, S. Li, Molecular architecture of the SARS-CoV-2 virus. *Cell* **183**, 730–738.e13 (2020).
45. R. Henderson, R. J. Edwards, K. Mansouri, K. Janowska, V. Stalls, S. M. C. Gobeil, M. Kopp, D. Li, R. Parks, A. L. Hsu, M. J. Borgnia, B. F. Haynes, P. Acharya, Controlling the SARS-CoV-2 spike glycoprotein conformation. *Nat. Struct. Mol. Biol.* **27**, 925–933 (2020).
46. G. J. Rocklin, T. M. Chidyausiku, I. Goreshnik, A. Ford, S. Houliston, A. Lemak, L. Carter, R. Ravichandran, V. K. Mulligan, A. Chevalier, C. H. Arrowsmith, D. Baker, Global analysis of protein folding using massively parallel design, synthesis, and testing. *Science* **357**, 168–175 (2017).
47. M. R. Gardner, L. M. Kattenhorn, H. R. Kondur, M. von Schaewen, T. Dorfman, J. J. Chiang, K. G. Haworth, J. M. Decker, M. D. Alpert, C. C. Bailey, E. S. Neale, C. H. Fellinger, V. R. Joshi, S. P. Fuchs, J. M. Martinez-Navio, B. D. Quinlan, A. Y. Yao, H. Mouquet, J. Gorman, B. Zhang, P. Poignard, M. C. Nussenzweig, D. R. Burton, P. D. Kwong, M. Piatak, J. D. Lifson, G. Gao, R. C. Desrosiers, D. T. Evans, B. H. Hahn, A. Ploss, P. M. Cannon, M. S. Seaman, M. Farzan, AAV-expressed eCD4-Ig provides durable protection from multiple SHIV challenges. *Nature* **519**, 87–91 (2015).
48. C. H. Fellinger, M. R. Gardner, J. A. Weber, B. Alfant, A. S. Zhou, M. Farzan, eCD4-Ig limits HIV-1 escape more effectively than CD4-Ig or a broadly neutralizing antibody. *J. Virol.* **93**, e00443–19 (2019).
49. L. Cao, I. Goreshnik, B. Coventry, J. B. Case, L. Miller, L. Kozodoy, R. E. Chen, L. Carter, A. C. Walls, Y.-J. Park, E.-M. Strauch, L. Stewart, M. S. Diamond, D. Veesler, D. Baker, De novo design of picomolar SARS-CoV-2 miniprotein inhibitors. *Science* **370**, 426–431 (2020).
50. E. Procko, R. Hedman, K. Hamilton, J. Seetharaman, S. J. Fleishman, M. Su, J. Aramini, G. Kornhaber, J. F. Hunt, L. Tong, G. T. Montelione, D. Baker, Computational design of a protein-based enzyme inhibitor. *J. Mol. Biol.* **425**, 3563–3575 (2013).

Acknowledgments: The Roy J. Carver Biotechnology Center at the University of Illinois assisted with flow cytometry and Illumina sequencing. **Funding:** This work was, in part, supported by NIH award R01AI129719 to E.P. **Author contributions:** E.P. designed the study and completed deep mutagenesis. K.K.C. purified proteins and tested BLI kinetics. K.K.C., K.K.N., and T.J.C.T. did flow cytometry. **Competing interests:** E.P. is an inventor on patent applications related to this work filed by the University of Illinois (number 62/989,976, filed 16 March 2020; number PCT/US2020/050903, filed 15 September 2020; number 63/089,895, filed 9 October 2020). E.P. and K.K.C. are cofounders of Orthogonal Biologics Inc. The authors declare that they have no other competing interests. **Data and materials availability:** All data needed to evaluate the conclusions in the paper are present in the paper and/or the Supplementary Materials. Additional data related to this paper may be requested from the authors.

Submitted 8 October 2020
Accepted 31 December 2020
Published 17 February 2021
10.1126/sciadv.abf1738

Citation: K. K. Chan, T. J. C. Tan, K. K. Narayanan, E. Procko, An engineered decoy receptor for SARS-CoV-2 broadly binds protein S sequence variants. *Sci. Adv.* **7**, eabf1738 (2021).

ScienceAdvances

An engineered decoy receptor for SARS-CoV-2 broadly binds protein S sequence variants

Kui K. ChanTimothy J. C. TanKrishna K. NarayananErik Procko

Sci. Adv., 7 (8), eabf1738. • DOI: 10.1126/sciadv.abf1738

Science Advances (ISSN 2375-2548) is published by the American Association for the Advancement of Science. 1200 New York Avenue NW, Washington, DC 20005. The title *Science Advances* is a registered trademark of AAAS.